Cellulose (2024) 31:6105–6122
https://doi.org/10.1007/s10570-024-05978-7

ORIGINAL RESEARCH

Rheological study of hybrid aqueous suspension of TEMPO-oxidized cellulose nanofibrils and graphene oxide

Iris Malnarič · Matjaž Krajnc · Urška Šebenik

Received: 26 February 2024 / Accepted: 23 May 2024 / Published online: 1 June 2024

Abstract The incorporation of graphene oxide (GO) into a nanocellulose matrix has attracted considerable attention due to the unique advantages of both components. This study focuses on investigating the viscoelastic and flow properties of hybrid aqueous suspensions (2.00 w/v%), composed of TEMPO-oxidized cellulose nanofibrils (TOCNF) and GO at different TOCNF/GO weight ratios. To adjust the elastic properties of the hybrid suspensions, calcium ions are introduced, varying the concentration systematically to study their effects on the hybrid network structure. All blends exhibit shear-thinning behaviour and demonstrate elastic, gel-like properties. Notably, in the absence of calcium ions, the enhancement of elastic properties is more pronounced at higher GO fractions. Conversely, with the introduction of calcium ions, the enhancement of elastic properties becomes particularly important at higher TOCNF fractions. For the quantitative evaluation of these enhancements, we employ the logarithmic mixing rule. Significant positive deviations from the predictions of the logarithmic mixing rule are ascribed to the complex, concentration-dependent arrangement of cellulose nanofibrils and GO liquid crystals in the aqueous suspension, coupled with ionic crosslinking induced by calcium ions. The study aims to contribute to the understanding of the rheological behaviour of the TOCNF/GO hydrogel, showing potential advancements in various applications.

I. Malnarič · M. Krajnc · U. Šebenik (✉)
Faculty of Chemistry and Chemical Technology,
University of Ljubljana, Večna pot 113, 1000 Ljubljana,
Slovenia
e-mail: urska.sebenik@fkkt.uni-lj.si

Graphical abstract

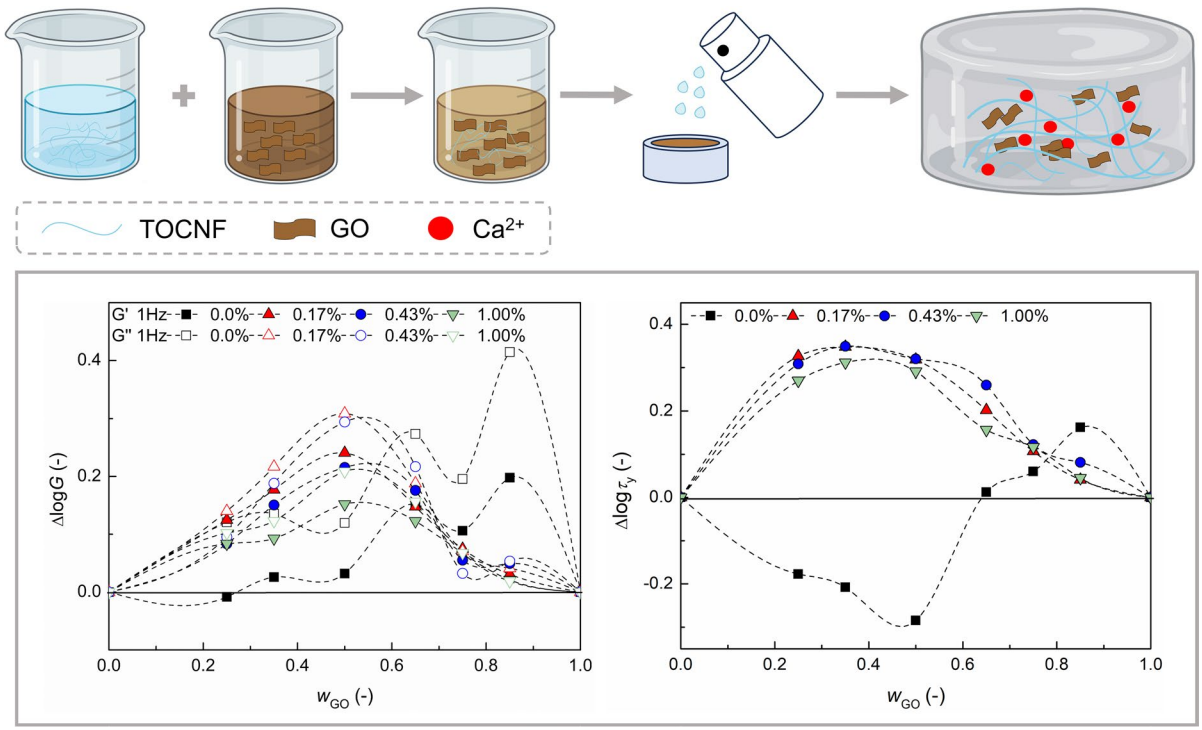

Keywords TEMPO-oxidized cellulose nanofibrils · Graphene oxide · Blending effect · Calcium ions · Hydrogel · Rheology

Introduction

Nanocellulose, featuring at least one dimension measuring less than 100 nm, is derived from an abundant, renewable and degradable cellulose resource. Over the last decades, nanocellulose has attracted significant attention due to its remarkable mechanical properties, high aspect ratio, and high crystallinity (Saito et al. 2007; Isogai et al. 2011). In addition, its biocompatibility, non-toxicity and biodegradability offer considerable potential for numerous applications (Curvello et al. 2019; Das et al. 2022). Various preparation methods employing distinct cellulose sources have been developed for producing diverse types of nanocellulose particles (Kargarzadeh et al. 2018), including cellulose nanocrystals (CNC), bacterial nanocellulose (BNC), and cellulose nanofibrils (CNF).

The 2,2,6,6-tetramethylpiperidine-1-oxyl (TEMPO) mediated oxidation is a well-established chemical pretreatment process used in production of highly fibrillated nanocellulose. In this procedure, the C6-primary hydroxy groups are selectively oxidized to sodium C6-carboxylate groups, introducing the negative charge on the surface of the fibrils (Araki et al. 2001; Xu et al. 2019). The process ensures the retention of the original cellulose crystallinity (Saito et al. 2007).

It has been reported that aqueous TEMPO-oxidized cellulose nanofibrils (TOCNF) suspension exhibit stable physical gel properties at concentrations exceeding 0.1 wt.% (Mendoza et al. 2018). The microstructure of TOCNF hydrogels, exhibiting elastic properties, can be described as a highly entangled and physically interconnected network with water-trapping properties. The microstructure properties are influenced by a combination of electrostatic interactions, hydrogen bonding, van der Waals forces, hydrophobic interactions, ionic interactions, and fibril

entanglements (Nechyporchuk et al. 2016; Curvello et al. 2019). TOCNF hydrogels exhibit thixotropic and shear thinning behaviour with a yield stress, which are more pronounced at higher cellulose concentration (Šebenik et al. 2019; Song et al. 2023; Xu et al. 2024). Studies have been conducted to comprehend the influence of nanocellulose particle properties, pH value and ionic strength of the aqueous phase on the rheological properties of hydrogels (Clasen and Kulicke 2001; Song et al. 2023). To enhance the mechanical properties of TOCNF hydrogels, which exhibit characteristics resembling those of a weak gel system (Šebenik et al. 2019), the capacity of TOCNF to form stronger ionic interactions with metal ions was exploited (Dong et al. 2013; Zhu et al. 2017; Xu et al. 2019; Kopač et al. 2021, 2022a). The ionic interactions between carboxylate groups on the surface of the cellulose nanofibrils and divalent metal ions, such as Ca^{2+}, cause TOCNF crosslinking and substantial improvements in elastic properties (Park et al. 2015; Khanjani et al. 2019; Kopač et al. 2021).

In our previous publication (Šebenik et al. 2019), we investigated the evolution of rheological properties in a hydrogel prepared from a commercially available freeze-dried TOCNF powder. The study revealed an increase in shear viscosity and elastic properties with concentration and aging time. Invisibly small clusters with significant swell-ability in water formed over time due to entanglements of nanofibers and physical interactions between them, i.e. not only hydrogen bonding but also van der Waals interactions and electrostatic repulsion. During aging, the clusters became larger due to water absorbance and the distance between them was reduced, which enhanced interactions between them. Solhi et al. (2023) reported that at the cluster–cluster interface, the surface bound water is located at the surface of the nanofibers, whereas in the same cluster, the confined bound water is present at the nanofiber interface. These findings offer valuable insights for diverse applications of nanocellulose hydrogels, particularly in the preparation of blends of high solids concentration.

Recently, layered nanomaterials with high aspect ratio and large surface area, such as nanoclays and graphene oxide (GO), have been incorporated into biopolymer hydrogels to further improve their properties and performance (Hao et al. 2022). In our previous study (Šebenik et al. 2020), TOCNF-Laponite hydrogel blends were prepared by blending TOCNF and Laponite suspensions, varying their ratio and total solids content. An increased elastic behaviour and a higher zero-shear viscosity were observed at a low Laponite fraction due to attractive interactions between carboxylic groups of the fibrils and the positively charged rims of Laponite nanodiscs. At higher Laponite fractions, edge-edge and face-face repulsion between Laponite nanodiscs became more and more important, resulting in a diminished elastic response, while at a very high Laponite fraction, disruption of the highly coordinated Laponite structure was observed in the presence of TOCNF.

Among graphene-based materials, which have received much attention due to their numerous advantages and unique properties (Yi et al. 2020), GO stands out for its ability to form stable aqueous suspensions owing to its hydrophilic nature and negative charge. The hydrophilicity arises from the presence of oxygen-containing functional groups, such as epoxy, hydroxyl, carbonyl, and carboxyl, while the negative charge results from dissociated carboxyl groups situated on the rims of GO (Konkena and Vasudevan 2014; Simsikova and Sikola 2017; Moraes et al. 2020). Aqueous GO suspensions have been categorized as isotropic liquids, nematic liquids as well as liquids in arrested states (glass or gels), depending on various factors, such as the aspect ratio of GO particles, pH value, and total solids concentration (Dan et al. 2011; Kumar et al. 2014; Del Giudice and Shen 2017; Nikzad et al. 2021). In our prior study (Malnarič et al. 2023), focused on investigating the rheological properties of suspensions containing GO particles with varying lateral dimensions and thicknesses, we demonstrated a strong dependence of the structural states of GO suspensions on both concentration and particle geometry. Concentrated GO suspensions exhibited viscoelastic behaviour typical for a suspension in an arrested state. Moreover, they exhibited pronounced shear thinning and thixotropic behaviour, characterized by a significant yield stress resulting from particle rotational restrictions, electrostatic attraction/repulsion, and nematic phase formation. However, a salt addition to GO suspension screens the electrostatic repulsion between GO particles, leading to agglomeration (Wang et al. 2016). It has been reported that divalent ions bind to the GO surface and bridge two individual GOs via complexation (Yang et al. 2016; Bayati and Fidalgo de Cortalezzi 2019). Konkena and Vasudevan (2014) showed that

at higher GO volume fractions and higher NaCl concentrations, the repulsive electrostatic interactions are screened, the attractive van der Waals forces dominate, and the suspension exhibits a nematic to columnar liquid crystal (LC) transition.

Since GO oxygen-containing functional groups as well its aromatic basal plane can strongly bind various organic and inorganic species through electrostatic, hydrogen bonding, van der Waals forces, hydrophobic and π-π stacking interactions (Cao et al. 2020; Raslan et al. 2020), it has been extensively explored as an adsorbent for the removal of pollutants from water and for controlled drug delivery systems with improved loading efficiency (Cao et al. 2020; Olate-Moya and Palza 2022). Through the same types of interactions, GO can be introduced into the nanocellulose matrix (Zhu et al. 2018, 2022; Wei et al. 2022), which can enhance the mechanical properties (Wei et al. 2022; Zhu et al. 2022), as well as the electrical (Valentini et al. 2013; Yi et al. 2020), optical (Mianehrow et al. 2020), antibacterial (Xia et al. 2019; Wei et al. 2022), and loading efficiency (Yi et al. 2020) of TOCNF hydrogels.

While some research work has provided empirical insights into the rheological characteristics of aqueous suspensions incorporating nanocellulose and GO, the focus is primarily on practical applications (Liu et al. 2019; Mianehrow et al. 2020). The investigations predominantly employ crystalline nanocellulose (Valentini et al. 2013; Singh Raghuwanshi et al. 2022; Shi et al. 2023), nanocellulose without ionic charge (Wang et al. 2021; Nguyen et al. 2022; Wei et al. 2022), and consistently use small amounts of GO (Jia et al. 2020; Shi et al. 2023). To the best of our knowledge, there is currently no reported comprehensive work on the rheological properties, in correlation with the hydrogel network characteristics, for the hybrid system containing TOCNF, GO, and calcium ions. Concentration-dependent arrangement of cellulose nanofibrils and GO liquid crystals in aqueous suspensions may form different complex network structures, and the incorporation of GO particles into a weak TOCNF hydrogel could improve its elastic properties and performance. Introduction of Ca^{2+} ions could facilitate connection between GO particles and TOCNF, further enhancing the elastic properties of the hybrid systems. It is expected that this enhancement will broaden the range of rheological properties and make the hybrid hydrogels suitable for a wider range of applications. Considering the complex network structures of the hybrid hydrogels, with or without Ca^{2+} ions, we hypothesize deviations from the mixing rule predictions. Therefore, this study systematically investigates the effects of blending TOCNF and GO suspensions (2.00 w/v%) at different weight ratios, specifically evaluating their effect on viscoelastic and flow properties. Furthermore, the study explores the effect of varying Ca^{2+} concentrations to develop hydrogel systems with superior elastic properties. The investigation employs rheological models and the logarithmic mixing rule for a quantitative evaluation of the experimental data. In addition, the study aims to thoroughly investigate the rheological behaviour associated with the hydrogel network characteristics. This understanding is crucial for tailoring the properties of the hydrogel and ultimately improving and expanding the applicability of this advanced hybrid system.

Experimental

Materials

Freeze-dried CNF modified by TEMPO (2,2,6,6-tetramethylpiperidine-1-oxyl), with the chemical formula $[(C_6H_{10}O_5)_x(C_6H_9O_4COONa)_y]$, was purchased from Cellulose Lab (Canada). According to the specifications given by the manufacturer, the purchased TEMPO-oxidized CNF powder was prepared from wood pulp. The nanofibril cellulose structure was web-like, with dimensions of $20-60$ nm in width and lengths of up to several microns. In our laboratory, the carboxylate content was determined to be 1.4 mmol g^{-1} by conductometric titration (Šebenik et al. 2019). The determined aldehyde content was 0.58 mmol/g solids. Single-layer GO material produced by a modified Hummer's method, with purity greater than 99 wt.%, was purchased from Cheap Tubes Inc. (Grafto, VT, USA). According to the manufacturer's data, the elemental composition of the purchased GO was 35–42% C, 45–55% O, and 3–5% H. The GO material had a particle thickness of 0.7–1.2 nm, determined by atomic force microscopy, and lateral particle dimensions of 300–800 nm, which was confirmed in our laboratory (Malnarič et al. 2023). The GO elemental composition was

determined to be 44.4% C, 52.5% O, and 2.3% H. The amount of carboxyl groups, determined by conductometric titration, was 1.9 mmol g^{-1}. Sodium azide (an assay of ≥ 99.5%), supplied by Sigma-Aldrich (St. Louis, USA), and calcium chloride supplied by Merck (Darmstadt, Germany), were used as received.

Sample preparation

2.00 w/v% aqueous TOCNF suspension was prepared by slowly adding demineralized water (with 0.02 w/v% of sodium azide) to the freeze-dried TOCNF powder. The non-homogeneous suspension was stirred at 750 rpm using a four-blade propeller stirrer. After 2 h, the suspension was treated in an ultrasonic bath for 1 h. The resulting suspension was stirred at 750 rpm at room temperature overnight and stored in the fridge at 4 °C for 30 days to establish a stable network structure (according to studies in (Šebenik et al. 2019)).

2.00 w/v% aqueous GO suspension was prepared by adding GO powder to demineralized water. The suspension was stirred at 750 rpm for 2 h using a four-blade propeller stirrer. Afterwards, the suspension was placed in an ultrasonic bath for 1 h. Finally, the obtained product was stored in the fridge at 4 °C for 24 h. The 2.00 w/v% concentration was chosen to achieve a significant viscoelastic response of the aqueous suspensions. It has been shown (Malnarič et al. 2023) that the aqueous suspension of the GO material used in this study has a nematic liquid crystallinity at 2.00 w/v%.

Aqueous TOCNF/GO suspensions were prepared by blending TOCNF and GO suspensions in different weight ratios using a four-blade propeller stirrer at 600 rpm for 3 h at room temperature. Then, the obtained blends were stored in the fridge at 4 °C for 24 h.

The suspensions were poured into a 1 mm thick 3D-printed mould with the diameter of the rheometer's measuring plate. $CaCl_2$ was dissolved in demineralized water at different concentrations (0.17, 0.43, and 1.00 w/v%). The prepared aqueous solution of calcium ions was sprayed onto the surface of the blends in the moulds. The sprayed volume of $CaCl_2$ solution was identical for all samples. The samples were kept in the fridge at 4 °C for 24 h to establish the final hydrogel structure.

Characterization

Before being examined, GO material and TOCNF powder were vacuum-dried for 24 h at room temperature in a vacuum dryer.

The zeta potential of TOCNF/GO blends in demineralized water at 25 °C was determined using the LitesizerTM 500 instrument (Anton Paar) and obtained by measuring the electrophoretic light scattering of the samples (Miller et al. 1991). To process the results, the Smoluchowski approximation was used (Esfahani et al. 2016; Smoluchowski 1921). The experiments were performed by using a concentration of 0.3 mg ml^{-1}. Average values of zeta potential for three replicates are reported.

The birefringence of TOCNF/GO blends was observed using a transmission-mode optical inverted microscope (Ti-U, Nikon) between crossed-polarizers. The blends were introduced into a rectangular glass capillary (0.01 × 0.10 mm) by capillary force and sealed with epoxy glue. The LC orientation of as prepared blends was measured using a full wave retardation plate.

Rheological investigation

Rheological measurements were performed on an Anton Paar Physica MCR 301 rheometer equipped with a 25 mm diameter crosshatched plate-plate geometry (PP25/P2) to reduce the wall-slip effect (Nechyporchuk et al. 2014), with a gap of 1 mm. To prevent the evaporation of water, a glass cover was used for the solvent trap. Each measurement was carried out three times at 25 °C.

The steady-state flow behaviour of the samples was determined by applying an increasing sequence of constant stress segments. The corresponding shear rate was measured in the shear rate range of 0.00001–1000 s^{-1}.

The flow curves were fitted using the Cross model (Eq. 1) (Cross 1965), which describes the rheological behaviour of a purely viscous fluid.

$$\eta = \eta_\infty + \frac{\eta_0 - \eta_\infty}{1 + (\lambda\dot{\gamma})^n} \quad (1)$$

η_0 and η_∞ represent the asymptotic values of viscosity at zero and infinite shear rates, respectively, n measures the shear rate dependence of viscosity in

the power law region, and λ is the characteristic time. The critical shear rate, denoted as $\dot{\gamma}_{cr}$, corresponds to the reciprocal value of the relaxation time λ. The Cross model and/or other models for purely viscous fluids have been often used to describe the properties of different GO suspensions (Konkena and Vasudevan 2014; Kumar et al. 2014; Naficy et al. 2014; Mypati et al. 2021) and TOCNF suspensions (Kopač et al. 2020, 2022b; Liao et al. 2020).

Since the investigated blends exhibit gel-like properties with a non-linear yield stress fluid behaviour, the viscoplastic Herschel-Bulkley model was also used to fit the flow curves (Eq. 2) (Herschel and Bulkley 1926):

$$\tau = \tau_y + K\dot{\gamma}^m \tag{2}$$

where τ is the shear stress, τ_y is the yield stress, K is the consistency index and m is the flow behaviour index.

Frequency sweep measurements were performed within the linear viscoelasticity range at constant strain (0.1%), defined by oscillatory stress sweep tests at 1 Hz. The oscillation frequencies varied from 100 to 0.1 rad s^{-1}.

The experimental data obtained by frequency sweep tests were fitted by generalized Maxwell (GM) model. Equations 3 and 4 describe the frequency dependence of the elastic and viscous moduli, respectively (Lapasin et al. 2017; Šebenik et al. 2019):

$$G' = G_e + \sum_{i=1}^{n} \frac{g_i \lambda_i^2 \omega^2}{1 + \lambda_i^2 \omega^2} \tag{3}$$

$$G'' = \sum_{i=1}^{n} \frac{g_i \lambda_i \omega}{1 + \lambda_i^2 \omega^2} \tag{4}$$

where n is the number of considered Maxwell elements, G_e is the equilibrium modulus when frequency approaches zero value, g_i is the relaxation modulus, and λ_i the corresponding relaxation time of the i^{th} Maxwell element, respectively. To reduce the degree of correlation between the adjustable parameters, the minimization procedure was performed by adopting the following recurrent constraint for the relaxation times: $\lambda_{i+1} = 10\lambda_i$. Based on the statistical method, n was chosen to minimize the product $\chi^2(n+2)$, where χ^2 is the sum of squared errors.

Results and discussion

Effect of graphene oxide fraction on rheological properties of blends

TOCNF/GO blends were prepared by blending 2.00 w/v% TOCNF and GO aqueous suspensions at various weight ratios (100:0, 75:25, 65:35, 50:50, 35:65, 25:75, 15:85, 0:100) to investigate the significance and impact of the GO fraction on the flow and viscoelastic properties of the blends. The experimentally determined zeta potential values for the blends in the above order were -49 mV, -50 mV, -43 mV, -45 mV, -44 mV, -42 mV, -40 mV, and -39 mV, respectively, indicating stable suspensions (Li et al. 2008). The GO fraction given in figures and text below is the GO weight fraction in the total solids content, including both TOCNF and GO. A detailed rheological characterization and description of structural properties of the 2.00 w/v% simple suspensions (TOCNF, GO) can be found in our previous publications (Šebenik et al. 2019; Malnarič et al. 2023). Measured and calculated values (using Cross and GM models) describing the rheological behaviour of TOCNF/GO blends are presented in Fig. 1.

The effect of the GO fraction on the flow behaviour was examined across eight decades of shear rates, up to 1000 s^{-1} (Fig. 1a). Notably, the GO flow curve displayed higher viscosity values than TOCNF throughout the entire shear rate range. The shear thinning behaviour, observed for TOCNF, GO, and their blends, is a characteristic feature of nanocellulose and GO suspensions with high solids content (Šebenik et al. 2019; Malnarič et al. 2023). This behaviour is attributed to the break-up of entangled TOCNF fibril network structures and alignment of the fibrils, as well as the alignment of GO particles and, at high GO concentrations, the breakage of GO nematic domains under the influence of the flow. At low GO fractions (0.50 and below), the flow curves of blends closely resembled that of TOCNF. However, with higher GO fractions (above 0.50), the influence of GO on the flow behaviour became more pronounced. Moreover, the η_0 values for blends with GO fraction of 0.75 and 0.85 surpassed the η_0 value of the simple GO suspension (Fig. 1f). Similar was observed for the τ_y values, quantitatively determined using Herschel-Bulkley model, which increased with increasing GO fraction. The higher the GO fraction, the larger the shear stress required to deform the blend structure to the point where it flows.

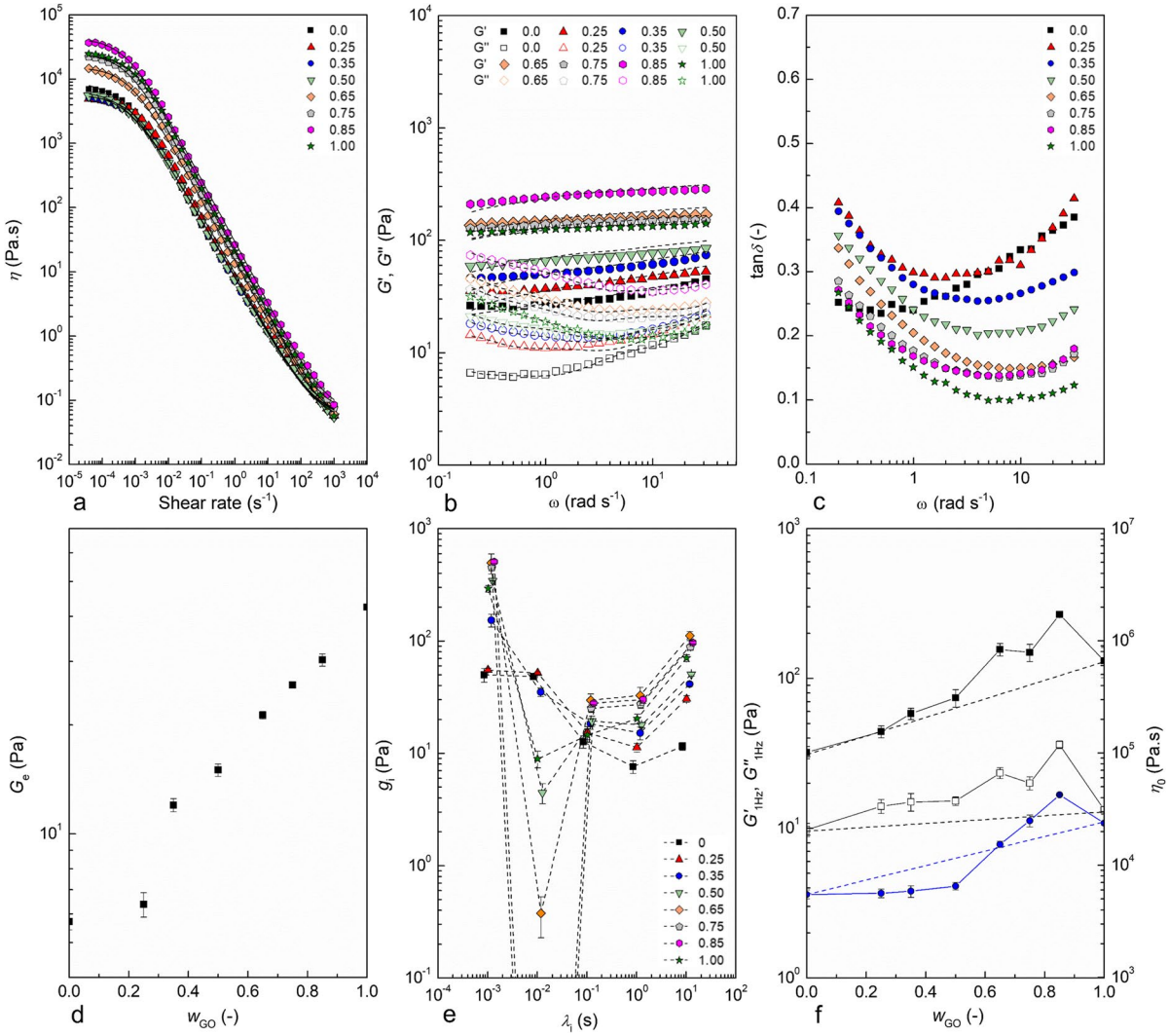

Fig. 1 **a** Flow curves of TOCNF/GO blends with different GO fractions. The solid lines represent Cross model fit. **b** Mechanical spectra of TOCNF/GO blends with different GO fractions. The dashed lines represent GM model fit of *G'* (filled symbols) and *G''* (empty symbols) experimental data. **c** Loss factor (tanδ) curves for TOCNF/GO blends with different GO fractions. **d** G_e dependency on GO fraction. **e** The relaxation time spectra for TOCNF/GO blends. **f** Storage modulus *G'* (filled squares) and loss modulus *G''* (empty squares) measured at 1 Hz vs GO fraction on the left axis. Zero-shear viscosity η_0 (circles) obtained by Cross model vs GO fraction on the right axis. The lines are drawn for easier reading of the results. The error bars show the standard deviation from the average of three measurements

The mechanical spectra depicted in Fig. 1b illustrate the dependence of storage (*G'*) and loss (*G''*) moduli on angular frequency. The *G'* values significantly exceeded the *G''* values and exhibited a slight frequency dependence across the angular frequency range from 0.1 to 100 rad s^{-1}, confirming the elastic character of the blends. It has been showed elsewhere (Šebenik et al. 2019; Malnarič et al. 2023) that both 2.00 w/v% TOCNF and 2.00 w/v% GO suspensions exhibit a typical viscoelastic behaviour characteristic of a suspension in an arrested state.

As the GO fraction increased, both *G'* and *G''* values also increased. Particularly at lower frequencies, a shift towards higher values of the loss modulus was observed. The blend with a GO fraction of 0.85 exhibited the highest moduli values, higher than GO

suspension. The same blend exhibited the highest viscosity values, which were higher than those of GO suspension (Fig. 1a).

The mechanical spectra were effectively described using the GM model, as shown in Fig. 1b, with the incorporation of five distinct relaxation times outlined in Eqs. (3) and (4). The equilibrium modulus (G_e), as illustrated in Fig. 1d, displayed a nearly linear progression corresponding to the increasing GO weight ratio (w_{GO}). The associated relaxation spectra show the significance of the frequency-dependent component of the moduli (Eqs. (3) and (4)). As depicted in Fig. 1e, the significance of the second Maxwell element markedly declined for blends with higher GO weight ratio (higher than 0.50). This suggests a notably reduced contribution of deformations associated with the relaxation time of around 0.01 s. In contrast, the highest g_i values corresponding to higher λ_i values were determined for GO and GO-rich blends.

The loss factor (tanδ) values (Fig. 1c) decreased with increasing GO fraction in the higher frequency range, confirming an increasing elastic character. Conversely, at lower frequencies, the tanδ values of blends decreased with increasing GO fraction but remained higher than those of GO and TOCNF suspensions, indicating a larger proportion of larger and non-reversible deformations. These findings further underscore the complex and nuanced interplay of elastic and viscous properties in the blends influenced by varying GO fractions.

In Fig. 1f, a summarized representation of the blending effect on viscoelastic and flow properties is provided. The figure illustrates moduli values at a selected frequency (1 Hz) and η_0 values for blends with different GO weight ratios. The lines in the figure connect the values of GO and TOCNF suspensions. Positive deviations of *G'* (indicative of elastic character) and *G''* (indicative of viscous character) values of blends from the respective lines indicate a synergistic effect of GO and TOCNF, especially at higher GO fractions. Conversely, η_0 values deviate positively and negatively from the line at higher and lower GO fractions, respectively. These deviations reflect the complex rheological behaviour influenced by the composition of the blends.

Effect of $CaCl_2$ concentration on rheological properties of blends

Having analysed the rheological behaviour of TOCNF/GO blends, we introduced calcium ions at various concentrations. This addition was implemented to develop a crosslinked hydrogel with improved elastic properties and to further enhance the structural features of TOCNF/GO blends.

In Fig. 2, the rheological measurements demonstrate the impact of blending TOCNF and GO suspensions at a $CaCl_2$ concentration of 0.17 w/v%. Upon the addition of $CaCl_2$, the shear-thinning behaviour was maintained (Fig. 2a). In comparison to blends without $CaCl_2$, η_0 values (Fig. 3a) and τ_y values exhibited a significant increase, particularly in GO-poor blends, where the values increased by more than two decades. Figure 3a consistently depicts similar patterns across all $CaCl_2$ concentrations, with a higher viscosity increase corresponding to higher $CaCl_2$ concentrations. Additionally, Fig. 3a reveals positive deviations from the lines (not shown in Fig. 3a) connecting the values of TOCNF and GO suspensions. These deviations suggest interactions between GO, TOCNF, and calcium ions enhancing the hydrogels' resistance to shear deformation.

The mechanical spectra of TOCNF/GO blends at a $CaCl_2$ concentration of 0.17 w/v% (Fig. 2b) show similar effect as the flow curves. The impact of calcium ion addition was more pronounced in GO-poor blends. The *G'* values significantly exceeded the *G''* values. However, with increasing TOCNF fraction, the *G''* values notably increased and showed a reduced frequency dependence.

The *G'* and *G''* values, measured at 1 Hz, are depicted in Fig. 3b as a function of GO fraction. The moduli values increased up to a GO fraction of 0.5; beyond this point, they decreased with an increasing GO fraction. Positive deviations from the lines connecting the values of TOCNF and GO suspensions (not displayed in the figure) were observed. In comparison to blends without $CaCl_2$, a significant increase in moduli values was noted. This increase was more prominent for blends with higher $CaCl_2$ concentrations.

The increasing elastic behaviour of the blends resulting from the addition of calcium ions is evident in the values of viscoelastic parameters (G_e and g_i) calculated by the GM model, as depicted in Figs. 3d, e, and f. The G_e increased by more than two decades for GO-poor suspensions and by one (in case of 1.00% $CaCl_2$) or less than one decade for GO-rich suspensions. The relaxation spectra of the blends (Fig. 3e), exhibiting a box-type distribution characteristic of a gel system, shifted to higher g_i values with increasing Ca^{2+} concentration. Similar shifts were observed in

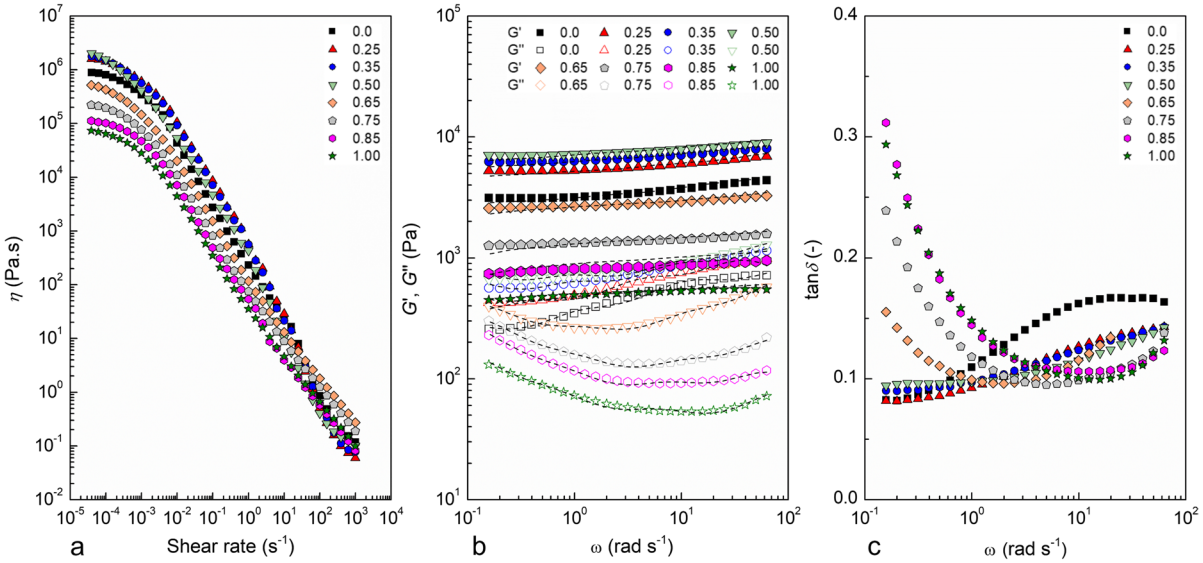

Fig. 2 Comparison of rheological behaviour of TOCNF/GO blends at a $CaCl_2$ concentration of 0.17 w/v%. **a** Flow curves of TOCNF/GO blends with different GO fractions. **b** Mechanical spectra of TOCNF/GO blends with different GO fractions. The dashed lines represent GM model fit of *G'* (filled symbols) and *G''* (empty symbols) experimental data. **c** Loss factor (tanδ) curves for TOCNF/GO blends with different GO fractions

the relaxation spectra of both TOCNF and GO alone. The influence of the TOCNF/GO ratio on the relaxation spectra at fixed Ca^{2+} concentration is depicted in Fig. 3f, where spectra of GO-poor blends are shifted to higher g_i values than the TOCNF spectrum.

Moreover, the lower tanδ values in Fig. 2c, compared to those in Fig. 1c, indicate an enhanced elastic character of TOCNF and blends upon the addition of Ca^{2+} to the system. On the other hand, the tanδ values of the GO suspension were not affected by the Ca^{2+} addition. Figure 3c demonstrates that at 1 Hz, the elastic character increased with both increasing GO fraction and $CaCl_2$ concentration. Conversely, at lower frequencies (0.1 Hz), the elastic character decreased with a higher GO fraction. It appears that at lower frequencies, the oscillation period was long enough to allow larger, irreversible deformations, particularly in GO-rich blends. The minimum in the tanδ curves (Fig. 2c), indicating the largest portion of reversible deformations, shifted to lower frequencies with an increasing amount of TOCNF.

Analysis of synergistic effects

The results presented in the previous chapter indicate that both the graphene oxide fraction and the addition of calcium ions have a significant impact on the structural organization of the TOCNF/GO blends, thereby influencing their rheological properties.

To better highlight the synergistic effects, a reference model was adopted, specifically the logarithmic mixing rule. The model equations (Eqs. (5)–(8)) predict the behaviour of a blend without interactions between the components affecting a rheological property (Grunberg and Nissan 1949; McAllister 1960):

$$log\eta_{0,mix} = w_{GO} log\eta_{0,GO} + (1 - w_{GO}) log\eta_{0,TOCNF} \quad (5)$$

$$log\tau_{0,mix} = w_{GO} log\tau_{0,GO} + (1 - w_{GO}) log\tau_{0,TOCNF} \quad (6)$$

$$logG'_{mix} = w_{GO} logG'_{GO} + (1 - w_{GO}) logG'_{TOCNF} \quad (7)$$

$$logG''_{mix} = w_{GO} logG''_{GO} + (1 - w_{GO}) logG''_{TOCNF} \quad (8)$$

Relative excess functions, representing the relative deviations from the predictions of the logarithmic mixing rule, were calculated using Eqs. (9)–(12), where the suffixes *ex* and *mix* denote the measured value and the value predicted by the logarithmic mixing rule, respectively.

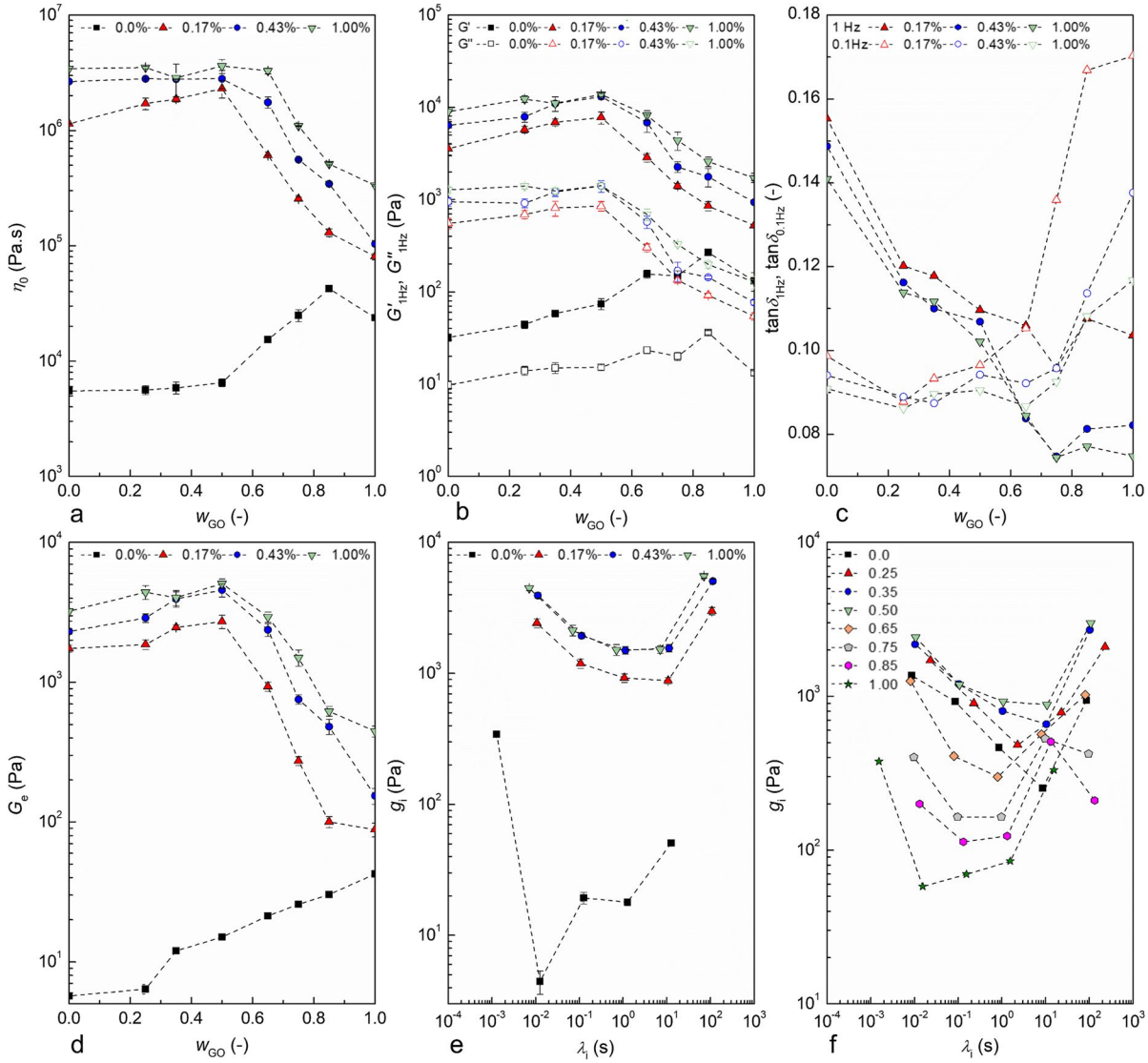

Fig. 3 **a** Zero-shear viscosity (η_0) obtained by Cross model vs GO fraction with and without the addition of calcium ions. **b** Storage modulus *G'* (filled symbols) and loss modulus *G''* (empty symbols) measured at 1 Hz vs GO fraction with and without the addition of calcium ions. **c** Loss factor (tanδ) curves measured at 1 Hz (filled symbols) and 0.1 Hz (empty symbols) vs GO fraction. **d** G_e dependency on GO fraction with and without the addition of calcium ions. The relaxation time spectra g_i-λ_i for **e** 0.50 GO fraction with the addition of calcium ions and **f** TOCNF/GO blends at a $CaCl_2$ concentration of 0.17 w/v%. The lines are drawn for easier reading of the results. The error bars show the standard deviation from the average of three measurements

$$\Delta log\eta_0 = \frac{log\eta_{0,ex} - log\eta_{0,mix}}{log\eta_{0,mix}} \quad (9)$$

$$\Delta log\tau_0 = \frac{log\tau_{0,ex} - log\tau_{0,mix}}{log\tau_{0,mix}} \quad (10)$$

$$\Delta logG' = \frac{logG'_{ex} - logG'_{mix}}{logG'_{mix}} \quad (11)$$

$$\Delta logG'' = \frac{logG''_{ex} - logG''_{mix}}{logG''_{mix}} \quad (12)$$

The calculated values of relative excess functions for moduli (at 1 and 0.1 Hz), zero-shear viscosity and yield stress, as a function of GO fraction, are shown in Fig. 4.

The observed deviations, i.e., the values of relative excess functions, from the ideal logarithmic mixing rule predictions can be explained by an altered suspension structure induced by blending. The blend structure is dictated by secondary interactions between GO and TOCNF, as well as interactions among them. According to the literature (Nechyporchuk et al. 2016; Curvello et al. 2019; Šebenik et al. 2019), the 2.00 w/v% TOCNF suspension can be described as a highly entangled and physically interconnected network with water-trapping properties. The suspension exhibits relatively high elastic properties, often referred to as a hydrogel, due to secondary

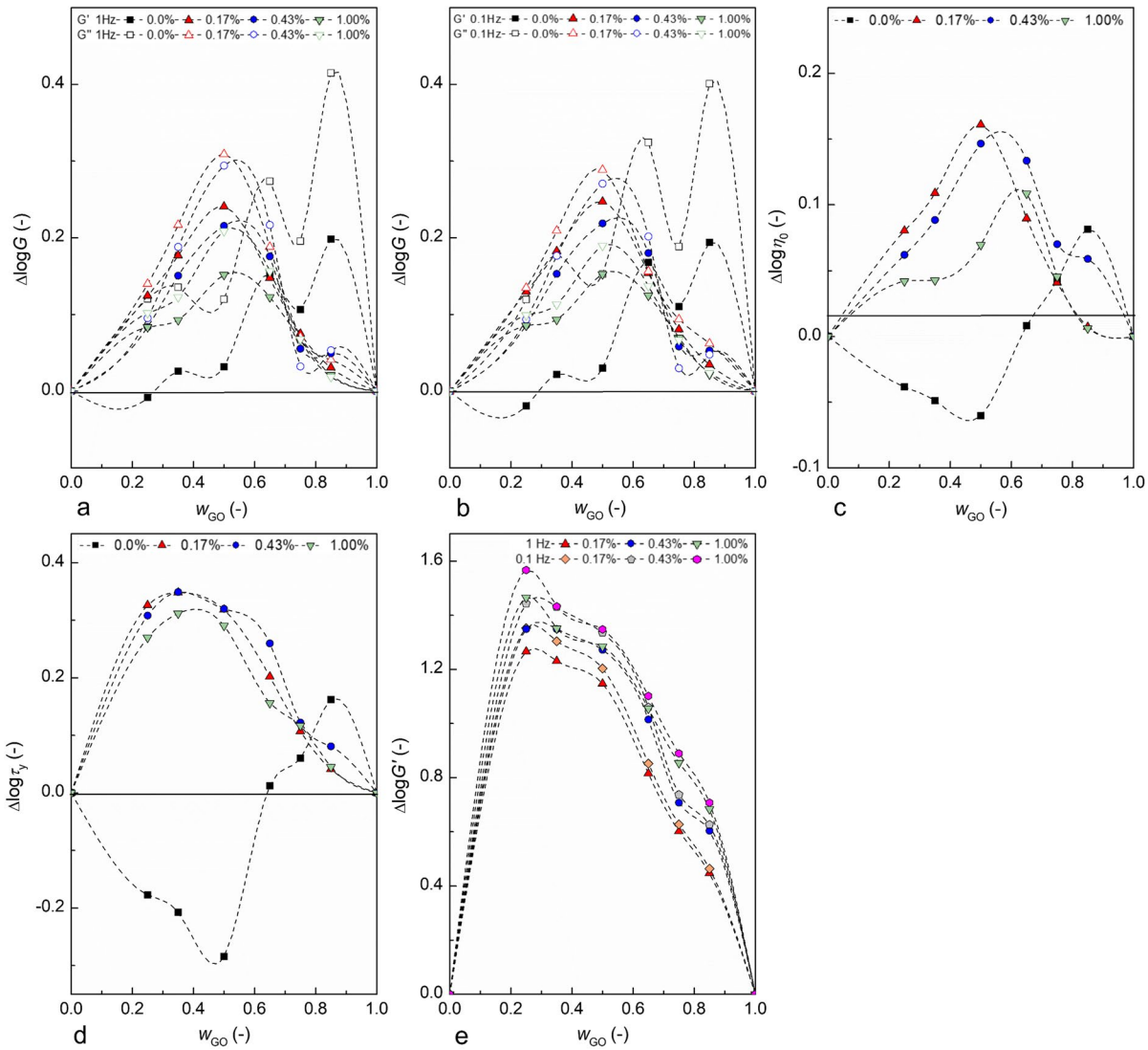

Fig. 4 Relative excess functions for **a** viscoelastic moduli at 1 Hz, **b** viscoelastic moduli at 0.1 Hz, **c** zero-shear viscosity, and **d** yield stress of TOCNF/GO blends vs GO fraction with and without the addition of calcium ions. In all panels, squares represent the measurement of blends without the addition of calcium ions, up-pointing triangles with a $CaCl_2$ concentration of 0.17 w/v%, circles with a $CaCl_2$ concentration of 0.43 w/v%, and down-pointing triangles with a $CaCl_2$ concentration of 1.00 w/v%. **e** The cumulative effect of blending and Ca^{2+} addition on relative excess function of *G'* at 0.1 and 1.0 Hz. The lines are drawn for easier data reading

interactions between fibrils, such as hydrogen bonds, van der Waals forces, and electrostatic interactions. Similar interactions, in addition to π-π interactions, contribute to the elastic properties of GO suspensions. In GO suspensions, electrostatic repulsion competes with attractive interactions originating from the unoxidized graphitic domains (Li et al. 2008; Vallés et al. 2014; Wang et al. 2016). Furthermore, earlier studies (Shu et al. 2016; Malnarič et al. 2023) have demonstrated that a 2.00 w/v% suspension of GO particles, with lateral dimensions ranging from 300 to 800 nm, exhibits a lyotropic LC phase due to rotational restrictions of the particles.

For TOCNF/GO blends without $CaCl_2$ (represented by the black square symbols in Figs. 4a–c), the following observations were made: at higher GO fractions (>0.50), the distribution of TOCNF in the GO matrix significantly contributed to both viscous and elastic behaviour ($G''_{ex} > G''_{mix}$ and $G'_{ex} > G'_{mix}$) of the blends. The viscous component of the modulus was more influenced than the elastic component. Furthermore, the zero-shear viscosity and yield stress values deviated positively from the mixing rule prediction ($\eta_{0,ex} > \eta_{0,mix}$) when the GO fraction exceeded 0.50. The enhanced properties of GO-rich blends, surpassing the predictions of the mixing rule, can be attributed to a combination of steric effects and attractive secondary interactions between the two materials, including hydrogen bonding, van der Waals interactions, and hinderance of the electrostatic repulsion between GO rims (Shim et al. 2017). In our interpretation, the presence of nanocellulose might induce the formation of larger GO domains and/or restrict the rotations of GO particles/domains, favouring nematic ordering (Narayan et al. 2016; Shim et al. 2017). This led to a substantial increase in all rheological parameters. As already mentioned in section above, the G', G'', η_0 and τ_0 values were even higher than those observed for the simple GO suspension. At this point, it might be speculated that the significantly reduced relevance of the second Maxwell element (as shown in Fig. 1e), associated with a relaxation time of around 0.01 s, for blends with a GO weight ratio of 0.5 and higher, might be attributed to restricted rotational deformation of GO particles. The relaxation time of approximately 0.01 s roughly corresponds to the calculated rotational relaxation time for a disk-like particle with a radius of around 150 nm in a diluted aqueous suspension, as determined using the Stokes–Einstein equation (Einstein 1956; Debye 1929).

The observed optical birefringence in Fig. 5 confirms the existence of GO nematic and TOCNF crystalline and amorphous (Isogai and Zhou 2019; Khanjani et al. 2019) domains in all blends. With increasing GO fraction, an enhanced organization into a nematic phase was observed (Fig. 5e–h). A full wave retardation plate (Fig. 6) was used to confirm the alignment along the flow direction due to surface tension and the effect of TOCNF domains on GO orientation. The arrows in Fig. 6g indicate the GO particle orientation induced by TOCNF, which was especially observed above 0.65 GO fraction.

At low GO fraction (up to 0.5 GO fraction), the GO distribution in the TOCNF hydrogel contributed significantly to the viscous behaviour ($G''_{ex} > G''_{mix}$), while the elastic behaviour followed the mixing rule prediction ($G'_{ex} \approx G'_{mix}$). However, the zero-shear viscosity and

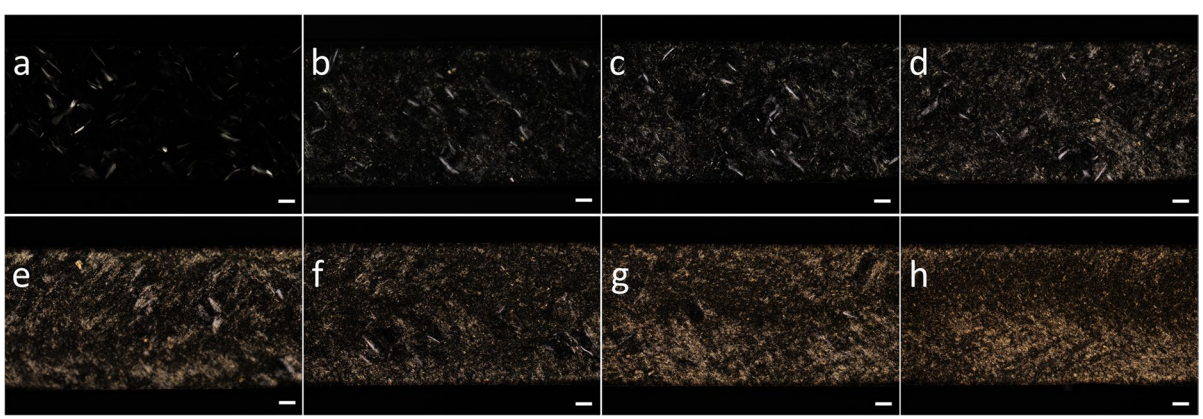

Fig. 5 Optical microscopy images obtained between crossed polarizers of different blends inside a capillary with **a** 0.0, **b** 0.25, **c** 0.35, **d** 0.50, **e** 0.65, **f** 0.75, **g** 0.85, and **h** 1.00 GO fraction. The scale bar represents 10 µm

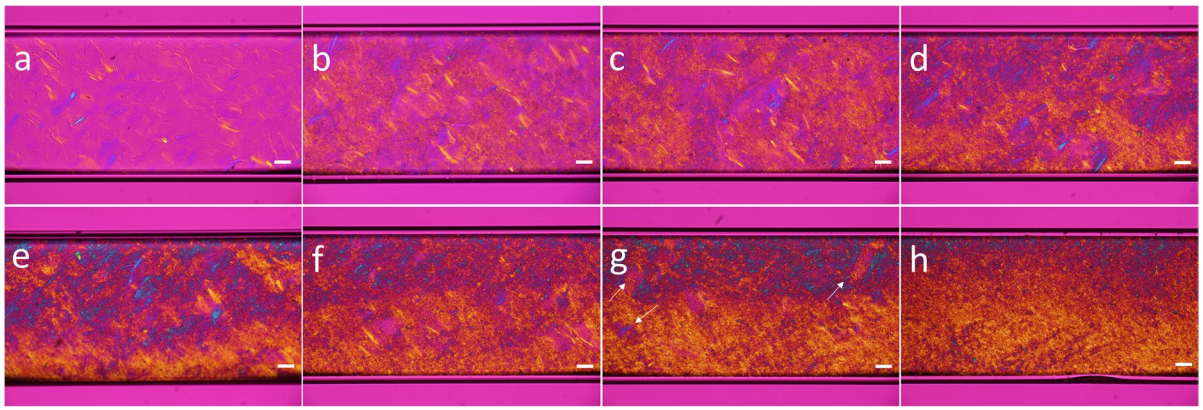

Fig. 6 Optical microscopy images using a full wave retardation plate of different blends inside a capillary with **a** 0.0, **b** 0.25, **c** 0.35, **d** 0.50, **e** 0.65, **f** 0.75, **g** 0.85, and **h** 1.00 GO fraction. The scale bar represents 10 µm

yield stress values showed negative deviations from the mixing rule prediction ($\eta_{0,ex} < \eta_{0,mix}$) up to 0.50 GO fraction. Similar was observed in Fig. 1f, suggesting considerably weaker secondary interactions than predicted by the mixing rule. Also, at lower frequencies (as already shown in Fig. 1c), the loss factor values of blends increased with the increasing TOCNF fraction and surpassed those of both GO and TOCNF suspensions, which indicated the occurrence of larger non-reversible deformations, requiring more time, such as substantial non-reversible fibril rearrangements. Indeed, this can be attributed to the disruption of the TOCNF hydrogel network structure in the presence of GO. GO might act as steric hindrance due to its random distribution of nematic domains within the TOCNF matrix (Fig. 6b–d). The hindrance could prevent, to some extent, nanocellulose fibrils from forming entanglements and engaging in physical interactions such as hydrogen bonding and van der Waals interactions among fibrils.

As shown previously, upon $CaCl_2$ addition, the *G'*, *G''*, η_0 and τ_0 values of TOCNF and GO suspensions increased. The observed increase of values for TOCNF suspension was considerably higher than that of the GO suspension. In a simple TOCNF suspension, calcium ions ionically crosslink the negatively charged carboxyl functional groups on cellulose D-glucose units, creating a network that strengthens the hydrogel (Kopač et al. 2020, 2021). Consequently, the importance of hydrogen bonding contribution to the hydrogel's elasticity is diminished (Kopač et al. 2022a).

On the other hand, in a simple GO suspension, the addition of salts screens the electrostatic repulsion between the negatively charged functional groups (Konkena and Vasudevan 2014), increasing the range of van der Waals forces and leading to agglomeration (Wang et al. 2016), i.e., GO platelets stacking. It has been reported, that the addition of calcium ions results in the formation of a GO–Ca^{2+}–GO complex (Bayati and Fidalgo de Cortalezzi 2019) and that cations can induce a nematic to columnar LC transition (Konkena and Vasudevan 2014).

When Ca^{2+} was added to TOCNF/GO blends, the positive effect of blending was observed for all blends, at all Ca^{2+}concentrations (Fig. 4). With increasing GO fraction, the relative excess function values first increased in GO-poor blends and then decreased in GO-rich blends. The relative excess function of the *G''* was more affected than that of the *G'* for all blends, both with maximum deviation at 0.5 GO fraction, at 1.0 and 0.1 Hz, as shown in Fig. 4a and b, respectively. Apparently, the maximum of $\Delta log\eta_0$ shifted toward higher GO fractions with increasing Ca^{2+} concentration (Fig. 4c), while $\Delta log\tau_0$ shifted toward lower GO fractions (Fig. 4d).

In blends containing a lower amount of GO, the primary interaction governing the structural arrangement of the blend is anticipated to be the Ca^{2+} bridging between the carboxyl groups of TOCNF. However, the positive synergistic effect between GO and TOCNF, confirmed by increasing positive $\Delta logG'$, $\Delta logG''$, $\Delta log\eta_0$ and $\Delta log\tau_0$ values with the increasing GO fraction, can be explained by the divalent cations bridging TOCNF and GO carboxylate groups. Therefore, the presence of Ca^{2+} appeared to overcome the

GO steric hindrance effect observed in blends without Ca^{2+}. Higher $\Delta logG''$ than $\Delta logG'$ values, at frequencies of 1.0 and 0.1 Hz, suggest that more energy than predicted by the mixing rule was required not only for reversible, elastic deformations but especially for viscous, irreversible deformations. At 1 Hz, the elastic contribution increased with the increasing GO fraction (Figs. 2c and 3c), as for the blends without Ca^{2+} (Fig. 1c). Conversely, after Ca^{2+} addition, at the frequency of 0.1 Hz, the loss factor values were low (<0.1) and unaffected by the GO fraction. This indicated that Ca^{2+} crosslinks significantly restricted larger non-reversible deformations, such as the disentanglements of TOCNF fibrils, and resulting rearrangements (including alignments and rotations) of GO particles. It is worth noting that at low frequencies, the loss factor values of blends without Ca^{2+} were even higher than those of simple compounds (Fig. 1c). The above-mentioned deformations (disentanglements of TOCNF fibrils between crosslinks and resulting GO rearrangements) might as well reflect as reduced viscosity at around 50 s^{-1} for GO-poor blends (Fig. 2a).

Interestingly, all relative excess function values ($\Delta log\eta_0$, $\Delta log\tau_0$, $\Delta logG'$, and $\Delta logG''$) at 1.00 w/v% $CaCl_2$ concentration were the lowest, which might be explained by a higher TOCNF crosslinking degree. This resulted in a diminished proportion of unreacted carboxyl groups available for bridging with GO. In simpler terms, as the concentration of $CaCl_2$ increased, the predictions of the mixing rule were more closely approached.

On the other hand, the introduction of Ca^{2+} ions in GO-rich blends, where GO rotation was already limited due to the presence of TOCNF, led to a further reduction in the rotation of GO particles, which was reflected in an additional increase in all rheological parameters (G', G'', η_0 and τ_0). The addition of Ca^{2+} ions not only screened the repulsive electrostatic interactions between GO rims but also established Ca^{2+} bridges, connecting GO particles with each other and with TOCNF. The significance of GO–Ca^{2+}–TOCNF interactions became more pronounced with the increasing TOCNF fraction, leading to higher values of relative excess functions.

At higher Ca^{2+} concentrations, the measured values of G', G'', η_0 and τ_0 increased due to the interactions described earlier. However, the impact of Ca^{2+} concentration on the relative excess functions was almost negligible at very high GO fractions (0.85 and above). The deviations from the predictions of the mixing rule were positive but relatively small. However, as mentioned above, the maximum $\Delta log\eta_0$ value shifted toward higher GO fractions with increasing $CaCl_2$ concentration, indicating the importance of GO–Ca^{2+}–TOCNF interactions.

What is intriguing is the behaviour of the loss factor at 0.1 Hz: the values of the loss factor increased (as shown in Fig. 3c), indicating a larger portion of larger and irreversible deformations, with the increase in GO fraction, reaching the highest value for the simple GO suspension. It's noteworthy that the opposite trend was observed in GO-rich blends without $CaCl_2$ (as depicted in Fig. 1c). In our view, this behaviour could be attributed to the GO complexation, leading to agglomeration and/or a transition from nematic to columnar LC phase. It is worth noting that it has been shown elsewhere (Jalili et al. 2014; Malnarič et al. 2023) that GO agglomeration leads to enhanced nematic phase formation. The shear-induced disruption and/or formation of agglomerated particles is an irreversible process (Esfahani et al. 2016; Del Giudice and Shen 2017; Gyarmati et al. 2022; Malnarič et al. 2023). However, the values of the loss factor decreased with increasing Ca^{2+} concentration and TOCNF fraction (Fig. 3c).

In Fig. 4e the cumulative effect of blending on the relative excess function of the elastic moduli is presented. The largest deviations from the mixing rule predictions were observed for GO-poor blends. These deviations imply that the interactions TOCNF–Ca^{2+}–TOCNF play a crucial role in influencing the elastic properties of the hydrogel.

Conclusions

A comprehensive investigation of the rheological properties of a hybrid system containing TOCNF, GO, and calcium ions was carried out. The results of the investigation correlate the rheological behaviour with the hydrogel network characteristics. For blends without the addition of Ca^{2+}, the values of moduli and zero-shear viscosity increased with increasing the GO fraction. Correspondingly, the loss factor values decreased, confirming the increasing elastic character of the blends after incorporation of GO particles into a weak hydrogel of cellulose nanofibrils. At low GO fractions, negative deviations of zero-shear viscosity and yield stress from the logarithmic mixing rule prediction were

ascribed to the disruption of the TOCNF hydrogel network structure in the presence of GO. The enhanced properties observed in GO-rich blends, surpassing the predictions of the mixing rule, and reaching a maximum at 0.85 GO fraction, were ascribed to the formation of larger GO domains and/or the restriction of their rotations, favouring nematic ordering, as confirmed by optical polarized microscopy. The addition of Ca^{2+} resulted in an improved elastic behaviour of the blends, as indicated by the values of viscoelastic parameters. Particularly, G_e increased by more than two decades for GO-poor blends and the relaxation spectra of the blends, exhibiting a box-type distribution characteristic of a gel system, shifted to higher g_i values with increasing Ca^{2+} concentration. Positive deviations from the linear mixing rule for zero-shear viscosity, yield stress and viscoelastic moduli were observed for all blends, at all Ca^{2+} concentrations. The positive effect of blending was explained by the divalent cations bridging TOCNF and GO carboxylate groups. The importance of GO–Ca^{2+}–TOCNF interactions became more pronounced with the increasing TOCNF fraction.

A wide range of complex rheological properties in this research provides valuable insights and contributes to a comprehensive understanding of the effects of blending on TOCNF and GO rearrangements. The findings offer essential knowledge for advanced applications such as hydrogels for controlled drug release, where the desired hybrid network structures may be controlled by varying the TOCNF/GO weight ratio and calcium ion concentration. Moreover, the ability to exploit the advantages of both components expands the potential applications of the hybrid TOCNF/GO hydrogel systems.

Acknowledgements This work was supported by the Slovenian Research and Innovation Agency (research core funding No. P2-0191). The authors thank I. Muševič and U. Jagodič for birefringence and liquid crystal orientation measurements (Figs. 5 and 6).

Author contributions Iris Malnarič: Conceptualization, Methodology, Formal analysis, Investigation, Visualization, Writing—original draft. Matjaž Krajnc: Writing—review & editing, Funding acquisition. Urška Šebenik: Conceptualization, Methodology, Supervision, Resources, Writing—review & editing.

Funding This work was supported by the Slovenian Research and Innovation Agency (research core funding No. P2-0191).

Data availability No datasets were generated or analysed during the current study.

Declarations

Ethical approval Not applicable.

Consent for publication All authors have consented to the publication of the submitted manuscript.

Competing interests The authors declare no competing interests.

References

Araki J, Wada M, Kuga S (2001) Steric stabilization of a cellulose microcrystal suspension by poly(ethylene glycol) grafting. Langmuir 17:21–27. https://doi.org/10.1021/la001070m

Bayati M, Fidalgo de Cortalezzi M (2019) Aggregation of graphene oxide in natural waters: role of solution chemistry and specific interactions. J Environ Eng 145:04019050. https://doi.org/10.1061/(asce)ee.1943-7870.0001561

Cao M, Shen Y, Yan Z et al (2020) Extraction-like removal of organic dyes from polluted water by the graphene oxide / PNIPAM composite system. Chem Eng J 405:126647

Clasen C, Kulicke WM (2001) Determination of viscoelastic and rheo-optical material functions of water-soluble cellulose derivatives. Prog Polym Sci 26:1839–1919. https://doi.org/10.1016/S0079-6700(01)00024-7

Cross MM (1965) Rheology of non-Newtonian fluids: a new flow equation for pseudoplastic systems. J Colloid Sci 20:417–437. https://doi.org/10.1016/0095-8522(65)90022-X

Curvello R, Raghuwanshi VS, Garnier G (2019) Engineering nanocellulose hydrogels for biomedical applications. Adv Colloid Interface Sci 267:47–61. https://doi.org/10.1016/j.cis.2019.03.002

Dan B, Behabtu N, Martinez A et al (2011) Liquid crystals of aqueous, giant graphene oxide flakes. Soft Matter 7:11154–11159. https://doi.org/10.1039/c1sm06418e

Das S, Ghosh B, Sarkar K (2022) Nanocellulose as sustainable biomaterials for drug delivery. Sens Int 3:100135. https://doi.org/10.1016/j.sintl.2021.100135

Debye P (1929) Polar molecules. J Soc. Chem Ind 48:1036–1037. https://doi.org/10.1002/JCTB.5000484320

Del Giudice F, Shen AQ (2017) Shear rheology of graphene oxide dispersions. Curr Opin Chem Eng 16:23–30. https://doi.org/10.1016/j.coche.2017.04.003

Dong H, Snyder JF, Williams KS, Andzelm JW (2013) Cation-induced hydrogels of cellulose nanofibrils with tunable moduli. Biomacromol 14:3338–3345. https://doi.org/10.1021/BM400993F

Einstein A (1956) Investigations on the theory of the Brownian movement. Dover, New York

Esfahani MR, Languri EM, Nunna MR (2016) Effect of particle size and viscosity on thermal conductivity enhancement of graphene oxide nanofluid. Int Commun Heat Mass Transf 76:308–315. https://doi.org/10.1016/j.icheatmasstransfer.2016.06.006

Grunberg L, Nissan AH (1949) Mixture law for viscosity. Nature 164:799–800. https://doi.org/10.1038/164799b0

Gyarmati B, Farah S, Farkas A, György S, Voelker-pop LM, Laszlo K (2022) Long-term aging of concentrated aqueous graphene oxide suspensions seen by rheology and Raman spectroscopy. Nanomater 12:916

Hao X, Yang S, Tao E, Li Y (2022) High efficiency and selective removal of Cu(II) via regulating the pore size of graphene oxide/montmorillonite composite aerogel. J Hazard Mater 424:127680. https://doi.org/10.1016/j.jhazmat.2021.127680

Herschel WH, Bulkley R (1926) Measurement of consistency as applied to rubber-benzene solutions. Am Soc Test Proc 26:621–633

Isogai A, Zhou Y (2019) Diverse nanocelluloses prepared from TEMPO-oxidized wood cellulose fibers: nanonetworks, nanofibers, and nanocrystals. Curr Opin Solid State Mater Sci 23:101–106. https://doi.org/10.1016/j.cossms.2019.01.001

Isogai A, Saito T, Fukuzumi H (2011) TEMPO-oxidized cellulose nanofibers. Nanoscale 3:71–85. https://doi.org/10.1039/c0nr00583e

Jalili R, Aboutalebi SH, Esrafilzadeh D et al (2014) Formation and processability of liquid crystalline dispersions of graphene oxide. Mater Horizons 1:87–91. https://doi.org/10.1039/c3mh00050h

Jia Y, Hu C, Shi P et al (2020) Effects of cellulose nanofibrils/graphene oxide hybrid nanofiller in PVA nanocomposites. Int J Biol Macromol 161:223–230. https://doi.org/10.1016/j.ijbiomac.2020.06.013

Kargarzadeh H, Mariano M, Gopakumar D et al (2018) Advances in cellulose nanomaterials. Cellulose 25:2151–2189. https://doi.org/10.1007/s10570-018-1723-5

Khanjani P, Kosonen H, Ristolainen M et al (2019) Interaction of divalent cations with carboxylate group in TEMPO-oxidized microfibrillated cellulose systems. Cellulose 26:4841–4851. https://doi.org/10.1007/s10570-019-02417-w

Konkena B, Vasudevan S (2014) Glass, gel, and liquid crystals: arrested states of graphene oxide aqueous dispersions. J Phys Chem C 118:21706–21713. https://doi.org/10.1021/jp507266t

Kopač T, Ručigaj A, Krajnc M (2020) The mutual effect of the crosslinker and biopolymer concentration on the desired hydrogel properties. Int J Biol Macromol 159:557–569. https://doi.org/10.1016/j.ijbiomac.2020.05.088

Kopač T, Krajnc M, Ručigaj A (2021) A mathematical model for pH-responsive ionically crosslinked TEMPO nanocellulose hydrogel design in drug delivery systems. Int J Biol Macromol 168:695–707. https://doi.org/10.1016/j.ijbiomac.2020.11.126

Kopač T, Abrami M, Grassi M et al (2022a) Polysaccharide-based hydrogels crosslink density equation: a rheological and LF-NMR study of polymer-polymer interactions. Carbohydr Polym 277:118895. https://doi.org/10.1016/j.carbpol.2021.118895

Kopač T, Ručigaj A, Krajnc M (2022b) Effect of polymer-polymer interactions on the flow behavior of some polysaccharide-based hydrogel blends. Carbohydr Polym 287:119352. https://doi.org/10.1016/j.carbpol.2022.119352

Kumar P, Maiti UN, Lee KE, Kim SO (2014) Rheological properties of graphene oxide liquid crystal. Carbon 80:453–461. https://doi.org/10.1016/j.carbon.2014.08.085

Lapasin R, Abrami M, Grassi M, Šebenik U (2017) Rheology of Laponite-scleroglucan hydrogels. Carbohydr Polym 168:290–300. https://doi.org/10.1016/j.carbpol.2017.03.068

Li D, Müller MB, Gilje S et al (2008) Processable aqueous dispersions of graphene nanosheets. Nat Nanotechnol 3:101–105. https://doi.org/10.1038/nnano.2007.451

Liao J, Pham KA, Breedveld V (2020) Rheological characterization and modeling of cellulose nanocrystal and TEMPO-oxidized cellulose nanofibril suspensions. Cellulose 27:3741–3757. https://doi.org/10.1007/s10570-020-03048-2

Liu P, Milletto C, Monti S et al (2019) Design of ultrathin hybrid membranes with improved retention efficiency of molecular dyes. RSC Adv 9:28657–28669. https://doi.org/10.1039/c9ra04435c

Malnarič I, Alič B, Krajnc M et al (2023) Rheological study of highly concentrated aqueous graphene oxide suspensions: the effects of concentration, particle lateral dimensions and number of layers per particle. Colloids Surf A Physicochem Eng Asp 675:132012. https://doi.org/10.1016/j.colsurfa.2023.132012

McAllister RA (1960) The viscosity of liquid mixtures. AIChE J 6:427–431. https://doi.org/10.1002/AIC.690060316

Mendoza L, Batchelor W, Tabor RF, Garnier G (2018) Gelation mechanism of cellulose nanofibre gels: a colloids and interfacial perspective. J Colloid Interface Sci 509:39–46. https://doi.org/10.1016/j.jcis.2017.08.101

Mianehrow H, Lo Re G, Carosio F et al (2020) Strong reinforcement effects in 2D cellulose nanofibril-graphene oxide (CNF-GO) nanocomposites due to GO-induced CNF ordering. J Mater Chem A 8:17608–17620. https://doi.org/10.1039/d0ta04406g

Miller JF, Schätzel K, Vincent B (1991) The determination of very small electrophoretic mobilities in polar and nonpolar colloidal dispersions using phase analysis light scattering. J Colloid Interface Sci 143:532–554. https://doi.org/10.1016/0021-9797(91)90286-H

Moraes LR d. C, Ribeiro H, Cargnin E et al (2020) Rheology of graphene oxide suspended in yield stress fluid. J Nonnewton Fluid Mech 286:104426. https://doi.org/10.1016/j.jnnfm.2020.104426

Mypati S, Sellathurai A, Kontopoulou M et al (2021) High concentration graphene nanoplatelet dispersions in water stabilized by graphene oxide. Carbon 174:581–593. https://doi.org/10.1016/j.carbon.2020.12.068

Naficy S, Jalili R, Aboutalebi SH et al (2014) Graphene oxide dispersions: tuning rheology to enable fabrication. Mater Horizons 1:326–331. https://doi.org/10.1039/c3mh00144j

Narayan R, Kim JE, Kim JY et al (2016) Graphene oxide liquid crystals: discovery, evolution and applications. Adv Mater 28:3045–3068. https://doi.org/10.1002/adma.201505122

Nechyporchuk O, Belgacem MN, Pignon F (2014) Rheological properties of micro-/nanofibrillated cellulose suspensions: wall-slip and shear banding phenomena. Carbohydr Polym 112:432–439. https://doi.org/10.1016/j.carbpol.2014.05.092

Nechyporchuk O, Belgacem MN, Pignon F (2016) Current progress in rheology of cellulose nanofibril suspensions. Biomacromol 17:2311–2320. https://doi.org/10.1021/acs.biomac.6b00668

Nguyen VT, Ha LQ, Nguyen TDL et al (2022) Nanocellulose and graphene oxide aerogels for adsorption and removal methylene blue from an aqueous environment. ACS Omega 7:1003–1013. https://doi.org/10.1021/acsomega.1c05586

Nikzad A, Akbari A, Grecov D (2021) Rheological properties of discotic nematic liquid crystals: graphene oxide dispersions study. Liq Cryst 48:1–14. https://doi.org/10.1080/02678292.2021.1897890

Olate-Moya F, Palza H (2022) Effect of graphene oxide on the pH-responsive drug release from supramolecular hydrogels. J Appl Polym Sci 139:51420. https://doi.org/10.1002/app.51420

Park M, Lee D, Hyun J (2015) Nanocellulose-alginate hydrogel for cell encapsulation. Carbohydr Polym 116:223–228. https://doi.org/10.1016/j.carbpol.2014.07.059

Raslan A, Saenz del Burgo L, Ciriza J, Luis Pedraz J (2020) Graphene oxide and reduced graphene oxide-based scaffolds in regenerative medicine. Int J Pharm 580:119226. https://doi.org/10.1016/j.ijpharm.2020.119226

Saito T, Kimura S, Nishiyama Y, Isogai A (2007) Cellulose nanofibers prepared by TEMPO-mediated oxidation of native cellulose. Biomacromol 8:2485–2491. https://doi.org/10.1021/bm0703970

Šebenik U, Krajnc M, Alič B, Lapasin R (2019) Ageing of aqueous TEMPO-oxidized nanofibrillated cellulose dispersions: a rheological study. Cellulose 26:917–931. https://doi.org/10.1007/s10570-018-2128-1

Šebenik U, Lapasin R, Krajnc M (2020) Rheology of aqueous dispersions of Laponite and TEMPO-oxidized nanofibrillated cellulose. Carbohydr Polym 240:116330. https://doi.org/10.1016/j.carbpol.2020.116330

Shi L, Hong G, Chen C et al (2023) Growth of spiral ganglion neurons induced by graphene oxide/oxidized bacterial cellulose composite hydrogel. Carbohydr Polym 311:120749. https://doi.org/10.1016/j.carbpol.2023.120749

Shim YH, Lee KE, Shin TJ et al (2017) Wide concentration liquid crystallinity of graphene oxide aqueous suspensions with interacting polymers. Mater Horizons 4:1157–1164. https://doi.org/10.1039/c7mh00624a

Shu R, Yin Q, Xing H et al (2016) Colloidal and rheological behavior of aqueous graphene oxide dispersions in the presence of poly(ethylene glycol). Colloids Surfaces A Physicochem Eng Asp 488:154–161. https://doi.org/10.1016/j.colsurfa.2015.10.006

Simsikova M, Sikola T (2017) Interaction of graphene oxide with proteins and applications of their conjugates. J Nanomedicine Res 5:00109. https://doi.org/10.15406/jnmr.2017.05.00109

Singh Raghuwanshi V, Varanasi S, Batchelor W, Garnier G (2022) Cellulose nanocrystals to modulate the self-assembly of graphene oxide in suspension. Mater Des 216:110572. https://doi.org/10.1016/j.matdes.2022.110572

Smoluchowski von M (1921) Elektrische Endosmose und Strömungsströme. In: Graetz L (ed) Handbuch der Elektrizität und des Magnetismus, J. A. Barth, Leipzig, pp 366–428

Solhi L, Guccini V, Heise K et al (2023) Understanding nanocellulose-water interactions: turning a detriment into an asset. Chem Rev 123:1925–2015. https://doi.org/10.1021/acs.chemrev.2c00611

Song Y, Kim B, Park JD, Lee D (2023) Probing metal-carboxylate interactions in cellulose nanofibrils-based hydrogels using nonlinear oscillatory rheology. Carbohydr Polym 300:120262. https://doi.org/10.1016/j.carbpol.2022.120262

Valentini L, Cardinali M, Fortunati E et al (2013) A novel method to prepare conductive nanocrystalline cellulose/graphene oxide composite films. Mater Lett 105:4–7. https://doi.org/10.1016/j.matlet.2013.04.034

Vallés C, Young RJ, Lomax DJ, Kinloch IA (2014) The rheological behaviour of concentrated dispersions of graphene oxide. J Mater Sci 49:6311–6320. https://doi.org/10.1007/s10853-014-8356-3

Wang M, Niu Y, Zhou J et al (2016) The dispersion and aggregation of graphene oxide in aqueous media. Nanoscale 8:14587–14592. https://doi.org/10.1039/c6nr03503e

Wang Z, Song L, Wang Y et al (2021) Construction of a hybrid graphene oxide/nanofibrillated cellulose aerogel used for the efficient removal of methylene blue and tetracycline. J Phys Chem Solids 150:109839. https://doi.org/10.1016/j.jpcs.2020.109839

Wei P, Wang L, Xie F, Cai J (2022) Strong and tough cellulose–graphene oxide composite hydrogels by multi-modulus components strategy as photothermal antibacterial platform. Chem Eng J 431:133964. https://doi.org/10.1016/j.cej.2021.133964

Xia M, Xie Y, Yu C et al (2019) Graphene-based nanomaterials: the promising active agents for antibiotics- independent antibacterial applications. J Control Release 307:16–31. https://doi.org/10.1016/j.jconrel.2019.06.011

Xu H, Liu Y, Xie Y et al (2019) Doubly cross-linked nanocellulose hydrogels with excellent mechanical properties. Cellulose 26:8645–8654. https://doi.org/10.1007/s10570-019-02689-2

Xu J, Wang P, Yuan B, Zhang H (2024) Rheology of cellulose nanocrystal and nanofibril suspensions. Carbohydr Polym 324:121527. https://doi.org/10.1016/j.carbpol.2023.121527

Yang K, Chen B, Zhu X, Xing B (2016) Aggregation, adsorption, and morphological transformation of graphene oxide in aqueous solutions containing different metal cations. Environ Sci Technol 50:11066–11075. https://doi.org/10.1021/acs.est.6b04235

Yi J, Choe G, Park J, Lee JY (2020) Graphene oxide-incorporated hydrogels for biomedical applications. Polym J 52:823–837. https://doi.org/10.1038/s41428-020-0350-9

Zhu C, Liu P, Mathew AP (2017) Self-assembled TEMPO cellulose nanofibers: graphene oxide-based biohybrids for water purification. ACS Appl Mater Interfaces 9:21048–21058. https://doi.org/10.1021/acsami.7b06358

Zhu C, Monti S, Mathew AP (2018) Cellulose nanofiber-graphene oxide biohybrids: disclosing the self-assembly and copper-ion adsorption using advanced microscopy and

ReaxFF simulations. ACS Nano 12:7028–7038. https://doi.org/10.1021/acsnano.8b02734

Zhu B, Wang K, Sun W et al (2022) Revealing the adsorption energy and interface characteristic of cellulose-graphene oxide composites by first-principles calculations. Compos Sci Technol 218:109209. https://doi.org/10.1016/j.compscitech.2021.109209